ACS APPLIED MATERIALS & INTERFACES

Research Article

www.acsami.org

High-Performance Poly(ethylene oxide)/Molybdenum Disulfide Nanocomposite Films: Reinforcement of Properties Based on the Gradient Interface Effect

Xiaming Feng,[†,‡] Weiyi Xing,*[,†] Hongyu Yang,[†,‡] Bihe Yuan,[†,‡] Lei Song,[†] Yuan Hu,*[,†,‡] and Kim Meow Liew[‡,§]

[†]State Key Laboratory of Fire Science, University of Science and Technology of China, Anhui 230026, P.R. China

[‡]Suzhou Key Laboratory of Urban Public Safety, Suzhou Institute for Advanced Study, University of Science and Technology of China, Suzhou, Jiangsu 215123, P.R. China

[§]Department of Architectural and Civil Engineering, City University of Hong Kong, Tat Chee Avenue, Kowloon, Hong Kong

Supporting Information

ABSTRACT: Herein, the molybdenum disulfide (MoS_2) was simultaneously exfoliated and noncovalently functionalized by ultrasonication in a Pluronic aqueous solution and then was used to prepare the poly(ethylene oxide) (PEO) based nanocomposite films. The homogeneous dispersion of MoS_2 and strong nanosheets/matrix interfacial adhesion were confirmed by representative electron microscopes. The considerable barrier action of the effective MoS_2 nanosheets obviously restricted the ordering of crystal lamellae and the motion of polymer chains and then resulted in the formation of the devastated spherocrystal structure and morphological alterations in the nanocomposites, which were confirmed by polarized optical microscopy and the high value of the glass transition temperature. Importantly, MoS_2 nanosheets hold great promise in reinforcing the thermal stability and mechanical property of polymer by increasing the effective volume of MoS_2 nanosheets. A substantial reinforcement effect of PEO/MoS_2 composite films was achieved: even at a relatively low loading level (0.9 wt %), 88.1% increase in Young's modulus, 72.7% increase in stress-at-failure, and 62.1 °C increment of the temperature corresponding to half weight loss were obtained. These significant reinforcements can be attributed to the gradient interface region, which could effectively transfer the stress from the weak polymer chains to the robust nanosheets, thus endowing the PEO/MoS_2 composite films with excellent properties.

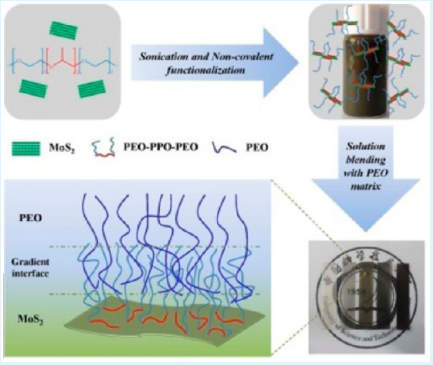

KEYWORDS: *poly(ethylene oxide), MoS_2 nanosheets, noncovalent functionalization, mechanical properties, thermal stability, gradient interface*

1. INTRODUCTION

In recent years, hexagonal MoS_2, a typical layered nonmaterial, has attracted an enormous amount of interest due to its wide range of applications.[1−3] Most of the efforts have been focused on the solid lubricants,[4,5] semiconductor characteristic,[6,7] and catalytic ability[8,9] of MoS_2. As with graphene, isolated inorganic sheets can be obtained from the bulk crystal via a variety of ways.[10−12] Similarly, a number of advances have been proved to exfoliate the MoS_2 nanosheets from the bulk materials,[7,13] especially the liquid-exfoliated method assisted with sonication in the preparation of polymer-based nanocomposites.[14,15]

Reinforcing polymer materials with two-dimensional nanosheets is becoming increasingly popular. These nanomaterials can efficiently enhance the physical properties of polymers for various kinds of engineering fields.[16,17] Typically, for the outstanding physical properties, graphene was regarded as an excellent candidate for the properties reinforcement of polymers.[18,19] However, for some applications, there is a requirement of effectively reinforced mechanical properties and thermal stability for polymeric materials while also maintaining their electrical insulation properties and the high dielectric constant. The high electric conductivity of graphene seems to be an impenetrable barrier to their utility in these applications such as electronic packaging and transmission lines.[17] Due to its semiconductor characteristics, the MoS_2 nanosheet may be an excellent substitute for graphene in the aforementioned applications. In the previous reports, the MoS_2 nanosheets have been proved to reinforce the polymer matrix obviously, owing to their inherent superior mechanical strength and thermal stability.[14,17,20] As with other nanofillers, the dispersion of MoS_2 nanosheets in matrices and the compatibility of polymer/MoS_2 play crucial roles in reinforcing polymer

Received: August 5, 2014
Accepted: June 1, 2015
Published: June 1, 2015

DOI: 10.1021/acsami.5b02312
ACS Appl. Mater. Interfaces 2015, 7, 13164−13173

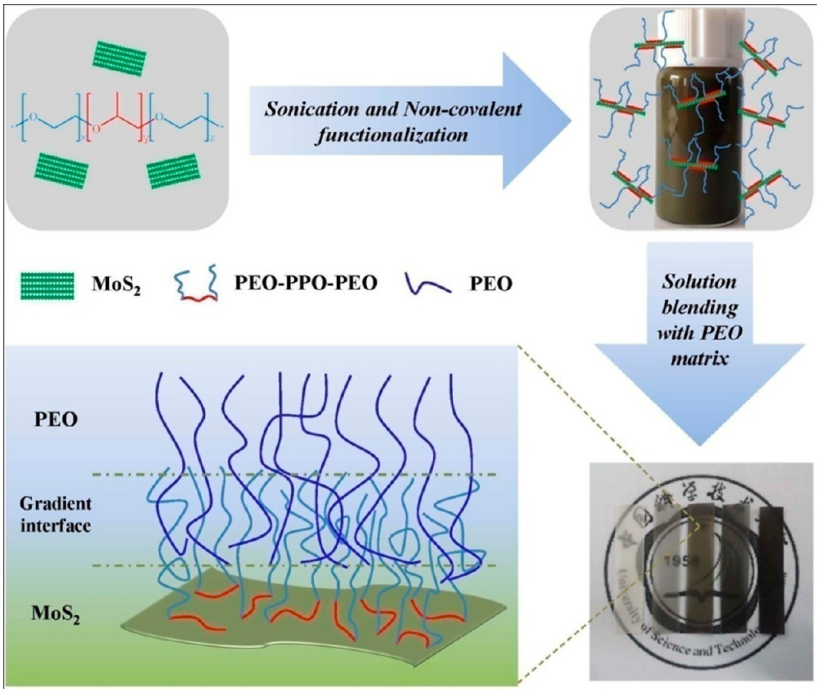

Figure 1. Procedure to prepare the homogeneously exfoliated MoS_2 dispersion and PEO/MoS_2 nanocomposite films.

composites. Unlike the highly defective and mechanically degraded MoS_2 nanosheets obtained from chemical exfoliation, the liquid sonication method assisted with green polymeric surfactant can produce the defect-free and well-dispersed nanosheets, which could facilitate processing on various occasions,[15] especially the fabrication of polymer nanocomposites.

Poly(ethylene oxide) is a hydrosoluble, semicrystalline, and biocompatible polymer which has been used in functional composites,[21] nanocomposite hydrogels,[22] electrospun nanofibers,[23] drug delivery systems,[24] etc. Over the past few years, various kinds of nanofillers were used to reinforce the thermal and mechanical properties and improve crystalline behavior of PEO materials. In particular, the nanosheets feature a large contact area by their two-dimensional geometry and are expected to show the nanoinclusion effects when they are homogeneously dispersed in polymer matrices. The structure−property relationships of PEO/graphene systems prepared by two techniques, liquid-phase blending and melt blending, were compared,[25] and the mechanical performance was obviously corresponding to the exfoliation extent and dispersion state of nanoflakes. Therefore, it is vital to achieve the surface functionalization of nanosheets for the satisfactory dispersion and substantial interfacial adhesion. On the basis of our previous work,[14,26] the noncovalent modification of nanosheets with green polymeric surfactant not only is environmentally friendly but also can ensure the considerable level of modification. The sufficient level of modification can efficiently lead to the uniform distribution of nanosheets in polymers and increase the effective interfacial volume, thus providing an effective stress transfer between polymers and nanoflakes and reinforcing the thermal and mechanical stability of nanocomposites.

On the basis of the discussion above, it is reasonable to believe the property enhancements for polymer composites heavily depend on the dispersion state of nanosheets and volume of interfacial region between the nanoflakes and polymer matrices. The proper surface modification of nanosheets will contribute to confine polymer chains on the MoS_2 nanosheets and enlarge the effective volume of MoS_2 nanosheets in the polymer matrices. Herein, we proposed to simultaneously exfoliate and noncovalently functionalize the MoS_2 by the sonication method with the aid of Pluronic surfactant, and the modified MoS_2 was used to fabricate the PEO/MoS_2 nanocomposite films. We anticipated that the addition of MoS_2 nanosheets could significantly reinforce the mechanical strength and thermal stability of PEO nanocomposites. The study of structure−property relationships will reveal the specific mechanism for the property enhancements and thus promote the development of polymer/MoS_2 nanocomposites.

2. EXPERIMENTAL SECTION

2.1. Materials. Powdered molybdenum disulfide (MoS_2, AP) was offered by Sinopharm Chemical Reagent Co., Ltd. (China). Pluronic L-64, with an average $M_n \sim 2.9$ kDa, was provided by Sigma-Aldrich. PEO with average $M_v \sim 100$ kDa, was supplied by Aladdin Industrial Inc. (China).

2.2. Exfoliation of MoS_2 in Pluronic Solution. Amounts of 0.1 g of MoS_2 powder and 50 mL of 10 wt % Pluronic aqueous solution were mixed in a 100 mL glass beaker upon ultrasonication to exfoliate MoS_2. The sonicating process lasted for 12 h and was agitated for 1 min every 20 min during this period to make the suspensions homogeneous. After centrifugation at 3500 rpm for 10 min, the uniform MoS_2 suspension had been obtained by collecting the supernatant. Finally, the MoS_2 was obtained by vacuum filtration of the stable MoS_2 dispersion, washing with deionized water repeatedly, and drying at 60 °C for 12 h in a vacuum oven.

2.3. Preparation of PEO/MoS_2 Nanocomposite Films. The PEO/MoS_2 nanocomposite films with different MoS_2 content (0.1, 0.3, 0.5, and 0.9 wt %) were fabricated. The MoS_2 obtained was ultrasonically dispersed in deionized water to yield a homogeneous dispersion. The PEO solution (20% w/v) was mixed with MoS_2 dispersion and sonicated for 0.5 h, and then the mixture was transferred into glass plates to mold the films. The nanocomposite

DOI: 10.1021/acsami.5b02312
ACS Appl. Mater. Interfaces 2015, 7, 13164−13173

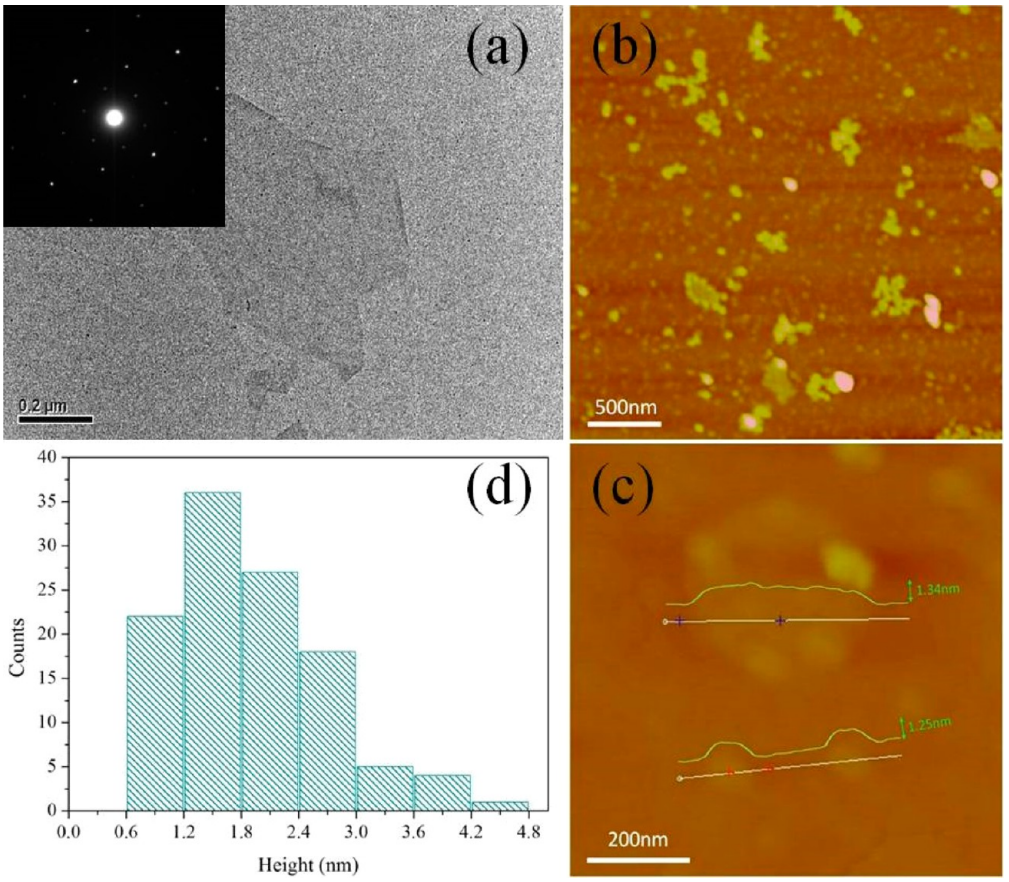

Figure 2. (a) TEM image of the exfoliated MoS_2. Inset shows the SAED pattern from the MoS_2 sheet. (b) Typical low-magnification and (c) high-magnification AFM image of the exfoliated MoS_2 marked with height profile. (d) Histograms for thickness of the exfoliated MoS_2.

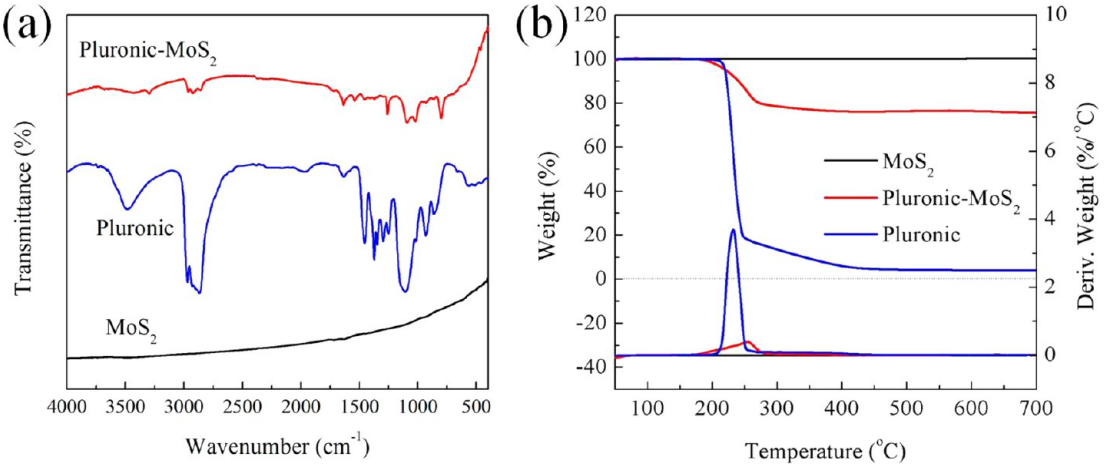

Figure 3. (a) FT-IR spectra and (b) TGA curves of bulk MoS_2, Pluronic, and Pluronic-functionalized MoS_2.

films were dried at 40 °C for 48 h and further dried at 80 °C for 5 h in vacuo.

2.4. Characterization. Fourier transform infrared (FT-IR) spectra were obtained from a Nicolet 6700 spectrometer (Nicolet Instrument Corporation, U.S.) by the KBr pellet technique.

X-ray diffraction (XRD) patterns were characterized by a TTR-III D/Max-Ra rotating-anode X-ray diffractometer (Rigaku Corporation, Japan) equipped with a Cu−K_α tube and a Ni filter (λ = 0.1542 nm).

The morphology of the exfoliated MoS_2 and ultrathin sections of PEO/MoS_2 nanocomposites were monitored by transmission electron microscopy (TEM) (JEM-2100F, Electron Optics Laboratory Co., Ltd. Japan), and the accelerating voltage was 200 kV. The atomic force microscopy (AFM) image was recorded in tapping mode by a DI Multimode V scanning probe microscope.

The fracture appearance of PEO nanocomposites was observed by an FEI Sirion 200 scanning electron microscope (SEM) at an acceleration voltage of 5 kV. The PEO nanocomposites were cryogenically fractured in liquid nitrogen and then sputter-coated with a conductive layer.

Optical morphology observations of the samples were obtained using an Olympus polarized optical microscope (POM). The PEO film clamped between two slides was heated from 20 to 100 °C at 20 °C min^{-1} on a hot stage and then cooled back at 2 °C min^{-1} to observe the growth of spherulites.

DOI: 10.1021/acsami.5b02312
ACS Appl. Mater. Interfaces 2015, 7, 13164−13173

Tensile testing was measured by a CMT4204 universal testing instrument (MTS Systems Co. Ltd., China) at a stretching speed of 50 mm min^{-1}.

Dynamic mechanical analysis (DMA) was studied by a DMA Q800 apparatus (TA Instruments Inc., U.S.) at a certain frequency of 10 Hz ranging from −120 to 60 °C at a heating rate of 5 °C min^{-1}.

The TA Q5000 thermoanalyzer instrument (TA Instruments Inc., U.S.) was used to complete the thermogravimetric analysis (TGA) of the samples under an air flow rate of 25 mL min^{-1} from 20 to 700 °C at a heating rate of 20 °C min^{-1}.

The crystallization property of the PEO films was monitored by a TA Q2000 differential scanning calorimetry (DSC) instrument (TA Instruments Inc., U.S.). After heating from 20 to 120 °C, the sample was held at 120 °C for 10 min and then cooled to 20 °C at 10 °C min^{-1}. The heating−cooling cycle was performed again, and the second heating curve was recorded.

3. RESULTS AND DISCUSSION

3.1. Exfoliation and Noncovalent Functionalization of MoS_2. The exfoliation and noncovalent functionalization of MoS_2 were processed by direct sonication of bulk MoS_2 powder with surfactant in water. The block copolymer surfactant Pluronic L-64 (PEO−PPO−PEO) was used in this study. This surfactant can obtain the optimal surface tension of solution to efficiently exfoliate and noncovalently functionalize MoS_2 nanosheets by the adsorption effect. Figure 1 schematically illustrates the preparation procedure of Pluronic-functionalized MoS_2 and PEO nanocomposite films with photographs at different stages. The Pluronic-MoS_2 can be well redispersed in water because of the hydrophilic PEO chain segment of Pluronic (Figure 1). The homogeneous dispersion obtained was blended with PEO matrix and subsequently dried to prepare the PEO/MoS_2 nanocomposite films.

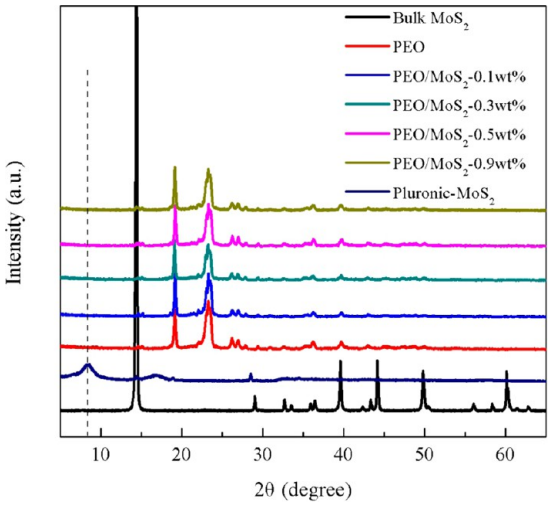

Figure 4. XRD patterns of bulk MoS_2, Pluronic-functionalized MoS_2, and PEO/MoS_2 nanocomposites.

Table 1. Crystallization Characteristics of PEO and Its Nanocomposites with Different MoS_2 Loadings

sample	T_c (°C)	T_m (°C)	ΔH_m (J/g)	X_c (%)
PEO	47.4	68.2	159.2	81.1
PEO/MoS_2-0.1 wt %	45.7	68.0	159.7	81.4
PEO/MoS_2-0.3 wt %	46.4	70.0	161.1	82.3
PEO/MoS_2-0.5 wt %	48.5	68.6	161.5	82.6
PEO/MoS_2-0.9 wt %	47.0	69.1	161.3	82.9

The morphology of MoS_2 nanosheets was observed with TEM and AFM techniques. Figure 2 shows the TEM and AFM results of exfoliated MoS_2 nanosheets. The TEM micrograph in Figure 2(a) reveals the presence of MoS_2 nanosheets in the diluted dispersion. The inset selected area electron diffraction (SAED) pattern confirms the hexagonal symmetry structure of the MoS_2. AFM images can directly provide sufficient information on the thickness and efficient exfoliation of the MoS_2 nanosheets. Figure 2(b) and (c) presents the different magnification AFM observations of the MoS_2 including the height profile. It is apparent that the lateral size of the MoS_2 nanosheets is tens or hundreds of nanometers wide in Figure 2(b). The thicknesses of the exfoliated MoS_2 nanosheets vary from 1.0 to 1.5 nm in Figure 2(c), which is fairly consistent with the thickness of the single-layer modified MoS_2 nanosheets by adsorbing polymeric surfactant.[27] Figure 2(d) is the histograms of the measured values for the thickness of the exfoliated MoS_2 nanosheets. It indicates that most of the MoS_2 nanosheets are 2−3 layers thick, and over 90% of them are 1−4 layers. The exfoliated MoS_2 nanosheet dispersion exhibits relatively narrow thickness distribution.

The MoS_2 nanosheets obtained were investigated with FT-IR and TGA for determination of successful surface modification. Figure 3(a) displays the FT-IR results of bulk MoS_2, Pluronic, and Pluronic-functionalized MoS_2. The absorption peaks at 2983 and 2845 cm^{-1} of Pluronic-functionalized MoS_2 can be assigned to the presence of $-CH_3$ and $-CH_2-$. The other absorption bands are similar to those of Pluronic, suggesting that the PEO−PPO−PEO molecules were adsorbed onto the MoS_2 nanosheets. Further evidence of the successful functionalization of MoS_2 nanosheets was obtained by TGA

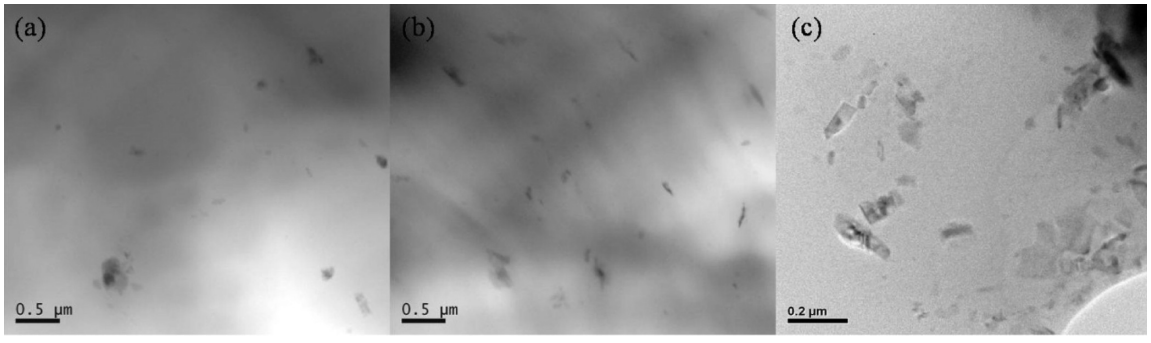

Figure 5. TEM images of ultrathin sections obtained from (a) PEO/MoS_2-0.3 wt %, (b) PEO/MoS_2-0.5 wt %, and (c) PEO/MoS_2-0.9 wt % nanocomposite films.

DOI: 10.1021/acsami.5b02312
ACS Appl. Mater. Interfaces 2015, 7, 13164−13173

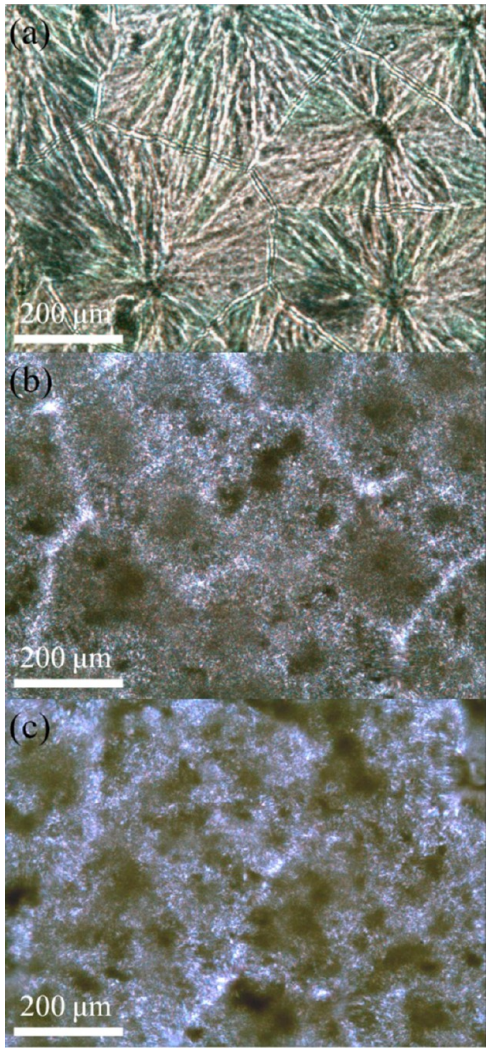

Figure 6. POM micrographs of (a) neat PEO, (b) PEO/MoS_2-0.3 wt %, and (c) PEO/MoS_2-0.9 wt % nanocomposite films.

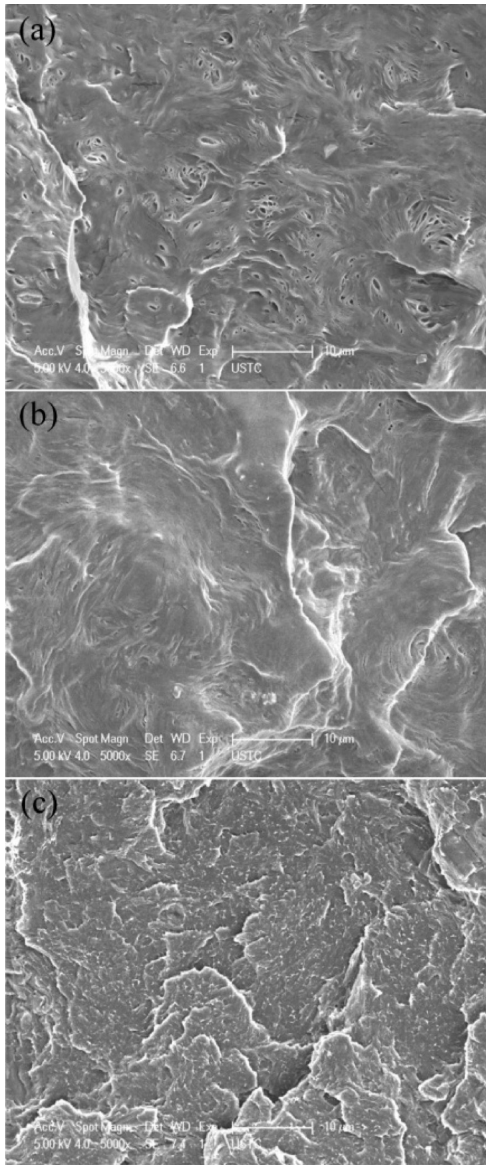

Figure 7. SEM images of the fractured sections of (a) neat PEO, (b) PEO/MoS_2-0.3 wt %, and (c) PEO/MoS_2-0.9 wt % nanocomposite films.

results, as shown in Figure 3(b). While bulk MoS_2 exhibits excellent thermal stability up to 700 °C in nitrogen atmosphere, the Pluronic displays a heavy weight loss from 200 to 300 °C. The TGA curve of Pluronic-functionalized MoS_2 exhibits a similar weight loss feature to that of Pluronic. According to the weight loss in the TGA curves, the content of polymeric surfactant in the modified MoS_2 is calculated to be approximately 23 wt %, suggesting a high degree of surface modification.

3.2. Characterization of PEO/MoS_2 Nanocomposites. As a powerful characterization method, XRD was usually performed to monitor the material structures. It can also partially evaluate the dispersion state of layered nanofillers in matrices. XRD patterns of the bulk MoS_2, modified MoS_2 nanosheets, and PEO/MoS_2 nanocomposites are compared in Figure 4. A broad, asymmetric, and weak (002) peak of Pluronic-MoS_2 is observed, different from that of the bulk MoS_2, indicating the destruction of the ordered crystalline in the direction of the *c*-axis of MoS_2 during the exfoliation process. Nevertheless, the expanded layer spacing of MoS_2 (from 0.62 to 1.16 nm) of the mentioned peak clearly confirms the intercalation of PEO−PPO−PEO molecules into the interlayer space of MoS_2 nanosheets. The characteristic peaks of MoS_2 are not observed in the XRD patterns of PEO/MoS_2 nanocomposites, confirming the homogeneous dispersion of MoS_2 nanosheets in PEO nanocomposite films.

To describe the dispersion state change in the PEO system with the increase of nanofiller content, TEM images of PEO/MoS_2 nanocomposite films are collected in Figure 5. It is clearly shown that most of the MoS_2 nanosheets with thin morphology are randomly dispersed in the PEO matrix without obvious aggregate, indicating the formation of exfoliated or intercalated structure. We speculate that the good dispersion of MoS_2 nanosheets benefits from a "gradient interface" mechanism, as shown in Figure 1, where the PEO chain segments in Pluronic act as the compatibilizer between the MoS_2 nanosheets and the PEO matrix. The formation of a gradient interface is essential for obtaining materials with improved properties.

3.3. Properties of PEO/MoS_2 Nanocomposites. *Crystallization Behavior.* The nonisothermal crystallization property of PEO nanocomposites was monitored with DSC. Figure S1 in the Supporting Information displays the second heating

DOI: 10.1021/acsami.5b02312
ACS Appl. Mater. Interfaces 2015, 7, 13164−13173

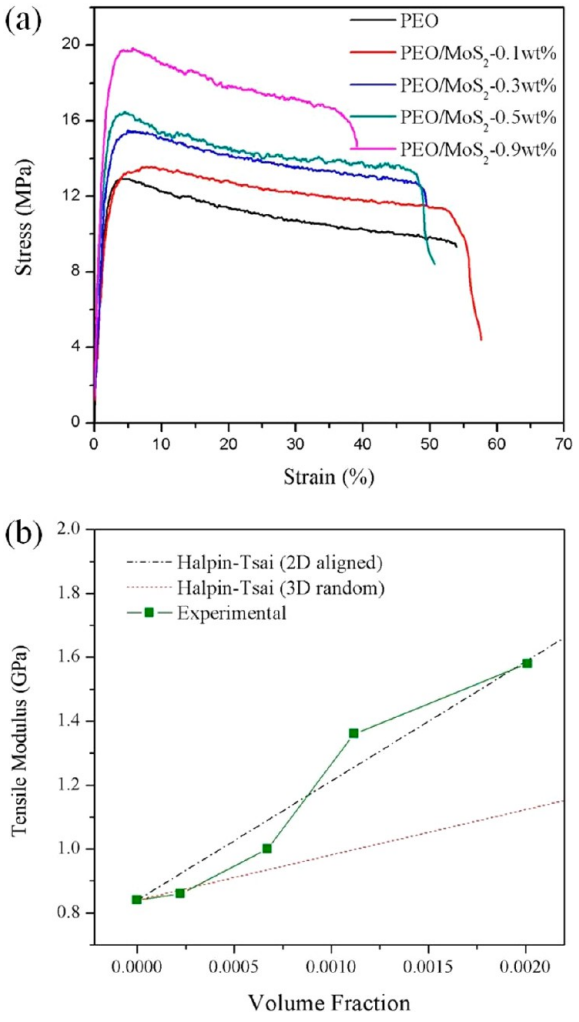

Figure 8. (a) Typical stress−strain curves of PEO and its nanocomposite films and (b) the experimental Young's modulus of the PEO/MoS_2 nanocomposites and theoretical curves of E_c and $E_{||}$ derived from the Halpin−Tsai model.

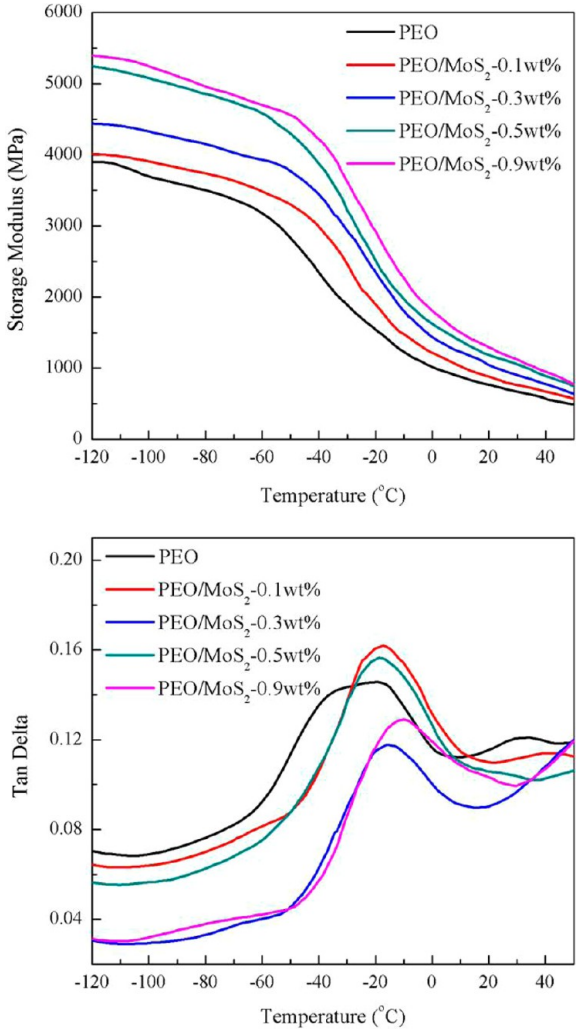

Figure 9. Storage modulus and tan δ as a function of temperature of PEO and its nanocomposites.

and cooling scans of PEO composite films. The degree of crystallization can be calculated by this equation

$$X_c = (\Delta H_m/\Delta H_0) \times 100\%$$

where ΔH_m is the melting enthalpy of PEO in films and ΔH_0 is 196.4 J g^{-1}.[28] As shown in Table 1, the enhancements in the T_c, T_m, and X_c of PEO nanocomposites are not marked, indicating that the addition of MoS_2 nanosheets exerts little effect on the nonisothermal crystallization process of the nanocomposites.

To further study the influence of the modified MoS_2 nanosheets on the spherocrystal structure of PEO, the polarized optical microscopy (POM) was employed to characterize the spherocrystal structure of PEO and its composites. As shown in Figure 6(a), the unambiguous spherulite morphology of neat PEO is observed. For the PEO nanocomposites, the MoS_2 nanosheets restrict the three-dimensional growth of spherulites, where the size of the spherulites decreases and the boundary becomes blurred in Figure 6(b) and (c) with increasing MoS_2 content. It is reasonable to conclude that the slight increase of the melting point and crystallinity of nanocomposites is attributed to the heterogeneous nucleation and favor crystallization of MoS_2 nanosheets by providing abundant crystal nucleus.

Study of Fractured Surfaces. In theory, after the exfoliation and surface noncovalent modification, the MoS_2 nanosheets will become more compatible with the PEO matrix. The compatibility and interfacial interactions of the modified MoS_2 with the polymer matrix were confirmed by the inspection of the fractured surface of PEO/MoS_2 nanocomposites by SEM. No obvious agglomerates and pull-out of MoS_2 nanosheets are observed in the SEM images of the fractured surface of PEO/MoS_2 nanocomposites, demonstrating that the MoS_2 nanosheets exhibit excellent dispersion and are embedded and tightly held in the PEO matrix. As stated above, the strong interfacial adhesion originates from the "gradient interface" between the MoS_2 nanosheets and PEO matrix, owing to the compatibilization effect of PEO chain segments in Pluronic. The strong interfacial adhesion can support a significant stress transfer and thus substantially reinforce the properties of polymer nanocomposites.

Interestingly, the well-defined lamellae and looming spherulite structure of neat PEO are observed in Figure 7(a).[29,30] However, these similar characteristics of the fractured surfaces of PEO nanocomposites become more difficult to identify in Figure 7(b) and (c). When the loading of MoS_2 is up to 0.9 wt %, the specific spherulite structure cannot be observed, and the fractured surface is considerably tough and

DOI: 10.1021/acsami.5b02312
ACS Appl. Mater. Interfaces 2015, 7, 13164−13173

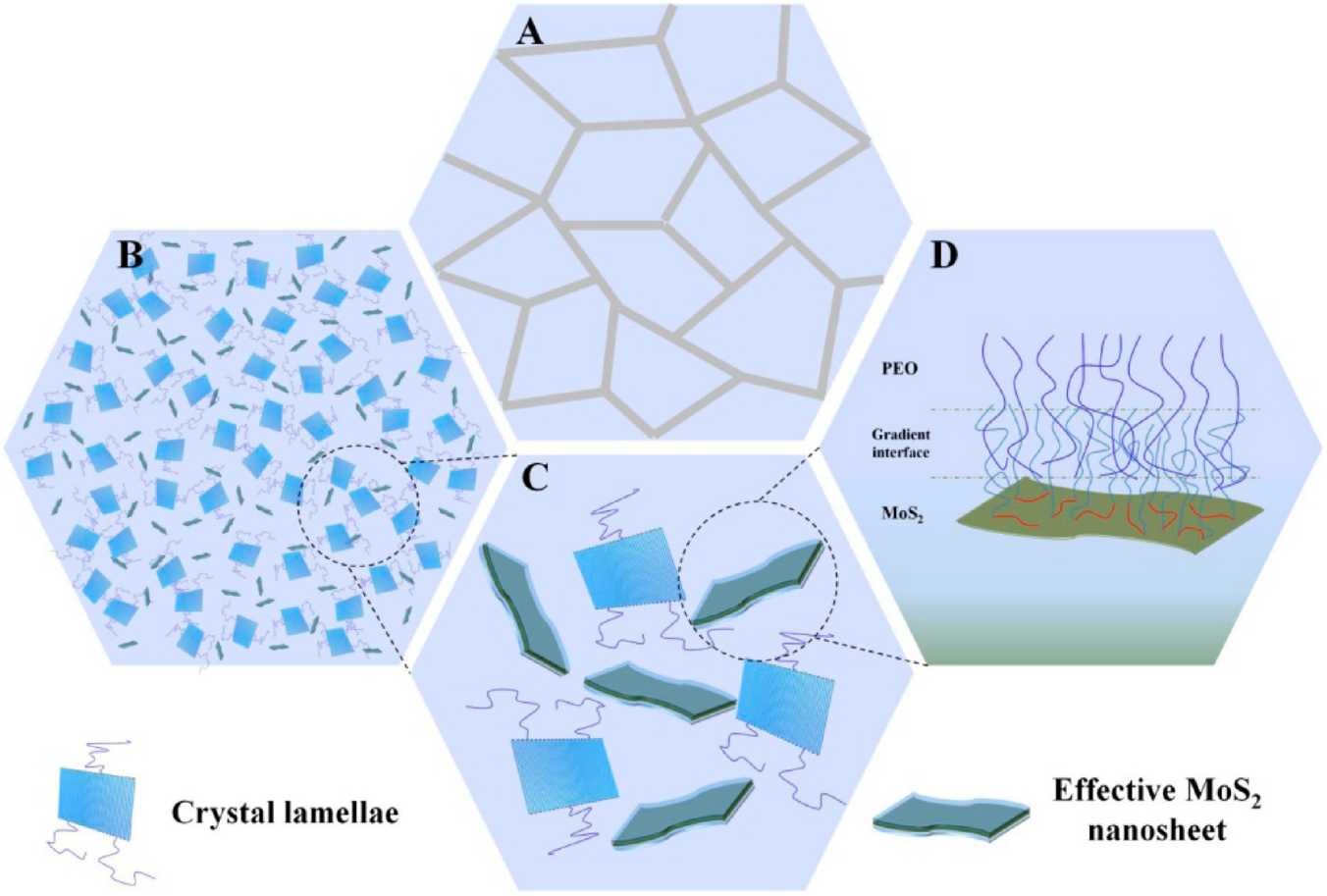

Figure 10. Proposed schematic of (a) large and distinct spherulites of neat PEO, (b) small and illegible crystal structure of PEO composites, (c) enlarged effective volumes of MoS_2 nanosheets, and (d) gradient interface between MoS_2 nanosheets and the PEO matrix.

irregular, indicating the destruction and imperfection of the spherulite structure of PEO and an efficient load transfer in composites.

Mechanical Reinforcing Effects. One of the most important property enhancements of polymer nanocomposites is mechanical properties by incorporating a fairly low additive amount of the nanomaterials.[12,15,17] Representative stress−strain curves of the PEO/MoS_2 nanocomposite films are plotted in Figure 8(a). Neat PEO displays a ductile fracture with a strain-at-failure of approximately 55% and yielding behavior. The addition of MoS_2 results in an obvious increase in the strain at yield point and an acceptable reduction in elongation at break. When the MoS_2 nanosheet content reaches 0.9 wt %, the Young's modulus, yield stress, and elongation at break of nanocomposites are increased by 88.1, 53.3, and 72.7%, respectively.

The Halpin−Tsai model is utilized to analyze the modulus of PEO/MoS_2 films.[31−33] E_c and $E_{\|}$ are denoted as the moduli of composites with randomly or unidirectionally dispersed MoS_2 nanosheets, respectively. They can be calculated by

$$E_c = E_m\left[\frac{3}{8}\frac{1+\eta_L\xi V_c}{1-\eta_L V_c} + \frac{5}{8}\frac{1+2\eta_T V_c}{1-\eta_T V_c}\right] \quad (1)$$

$$E_{\|} = E_m\left[\frac{1+\eta_L\xi V_c}{1-\eta_L V_c}\right] \quad (2)$$

$$\eta_L = \frac{(E_g/E_m)-1}{(E_g/E_m)+\xi} \quad (3)$$

$$\eta_T = \frac{(E_g/E_m)-1}{(E_g/E_m)+2} \quad (4)$$

$$\xi = 2\alpha_g/3 = 2l_g/3t_g \quad (5)$$

where E_g and E_m refer to Young's modulus of MoS_2 (300 GPa[34]) and PEO (0.84 GPa). l_g, t_g, and V_c stand for the length, thickness, and volume fraction of the MoS_2 in the composites. These two theoretical and the actual moduli of the PEO composite films are compared in Figure 8(b). Obviously, the real moduli of the PEO composites are close to the curve of E_c, which demonstrates that the MoS_2 sheets are randomly dispersed in PEO composites principally. It is noteworthy that the sudden increase in moduli of above 0.5 wt % loading can be attributed to morphological alterations of crystal and fundamental structural reorganization at the molecular level. The detailed discussion will be presented in the following section.

Dynamic Mechanical Analysis. The effect of MoS_2 inclusion on the viscoelastic properties of PEO nanocomposites was evaluated by DMA. Figure 9 depicted storage modulus and tan δ vs temperature curves of PEO films. The storage modulus of PEO films is dramatically improved as the MoS_2 content increases. The maximum increase in the storage modulus of nanocomposites is up to 38.3% at −120 °C and 92.7% at −30

DOI: 10.1021/acsami.5b02312
ACS Appl. Mater. Interfaces 2015, 7, 13164−13173

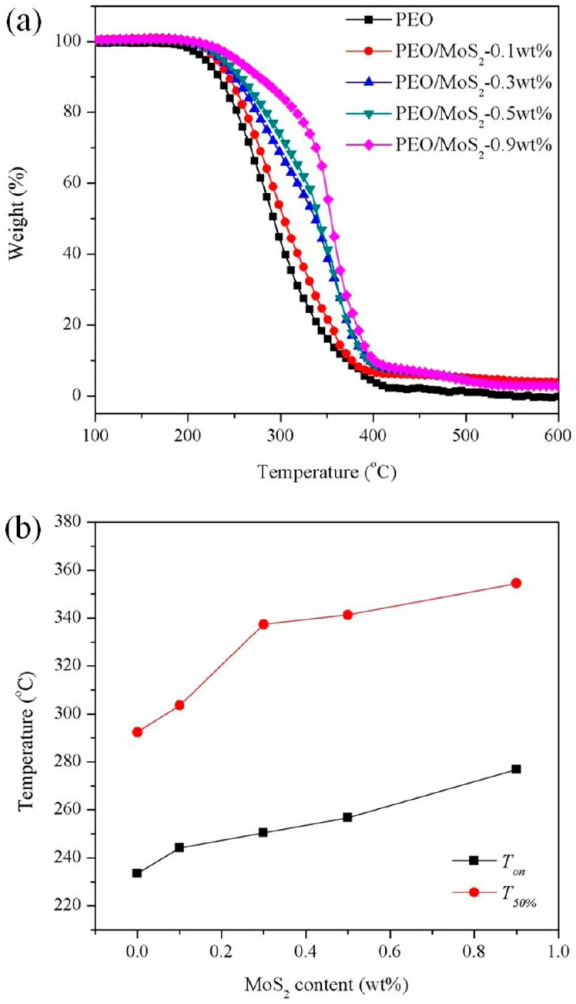

Figure 11. (a) TGA curves of PEO nanocomposites and (b) plots of degradation temperature vs MoS_2 contents.

°C at the 0.9 wt % loading of MoS_2 ,respectively, indicating the reinforcement effect by the inclusion of MoS_2 nanosheets. It is general to regard the temperature corresponding to the peak of tan δ as the glass transition temperature (T_g).[14] In comparison to neat PEO, the T_g values of the composite films all shift to higher temperature. Particularly, the 9.5 °C increase in T_g is achieved in PEO/MoS_2-0.9 wt %. These obvious enhancements in T_g at extremely low filler loadings support the presence of the gradient interfacial region between MoS_2 nanosheets and the PEO matrix by nanoconfinement effects.

On the basis of the analysis above, we speculate a relatively reliable schematic illustration of the structure−property relationship in Figure 10. Compared to the large and distinct crystalline spherulites of neat PEO in Figure 10(a), the spherulite structures of the PEO nanocomposites are more difficult to identify in Figure 10(b). In general, a decreased spherulite size will reduce the tensile and yield strengths but increase the elongation at break. However, the efficient reinforcement of mechanical properties for PEO composites is obtained in this investigation. This phenomenon can be explained by the two counter-balancing forces of nanofillers mentioned in the previous report.[35] Herein, the reinforcing effects of the MoS_2 nanosheets obviously prevail over the negative effects from the nucleating of MoS_2 filler. Furthermore, the spherulites with reduced size can improve the impact strength of PEO nanocomposites, which will be studied in our future work.

The dramatic mechanical property improvements of PEO composite films can be attributed to the robust interface adhesion in PEO/MoS_2 composites. The enhancements in Young's modulus and the value of T_g are usually employed to evaluate the interface quality between the nanofillers and polymer matrix. The considerably increased Young's modulus of PEO composites reveals the presence of enlarged effective volumes of MoS_2 nanosheets, as depicted in Figure 10(c). The reinforcement in tensile strength is positively related to the effect of interface volume, which indicates that maximizing the effective volume of nanofillers will optimize the mechanical stress of nanocomposites.[36] After the exfoliation and noncovalent modification of MoS_2, the effective volume of MoS_2 nanosheets in the PEO matrix is obviously increased, although the exact mechanism is still unclear. The recent reports concerning the nanoconfinement effect provide some insights. It can scrupulously speculate that the enlargement of the effective volume of MoS_2 nanosheets can be assigned to two points: the crystalline coating on the MoS_2 surface or the interfacial volume occupied by the modified groups. In this paper, the above two points both can be originated from the formation of gradient interface between the nanosheets and polymer matrices at the molecular level in Figure 10(d). This interface can confine the PEO molecular chains to form the nanocrystal or nanoconfined interfacial regions on the surface of nanosheets. Due to the stiffness of the nanocrystal and the nanoconfined interfacial regions, the mismatch between the stiff nanosheets and soft polymers can be easily overcome and result in the formation of the effective stress transfer region in polymer nanocomposites. In conclusion, the incorporation of noncovalently functionalized MoS_2 nanosheets in the PEO matrix results in the morphological alterations of crystal and fundamental structural reorganization at the molecular level, especially in enlarging the effective volumes of MoS_2 nanosheets and forming the gradient interfaces between nanosheets and matrices. The gradient interfaces can restrict the motion of polymer chains heavily by the molecular level entanglement and provide an effective load transfer region; therefore, the mechanical strength of PEO composite films is significantly improved.

Thermal Stability. As is well-known, incorporating inorganic layered materials usually results in an effective enhancement in thermal stability of polymer composites.[37,38] TGA plots of PEO samples are depicted in Figure 11(a). The temperatures corresponding to 10 wt % weight loss (T_{on}) that are usually used to evaluate the onset degradation temperature of polymer and the temperature at half weight loss ($T_{50\%}$) are recorded in Figure 11(b). Both pure PEO and its nanocomposites follow a main weight loss stage corresponding to the thermal degradation of PEO backbones. Compared to pure PEO, the addition of as low as 0.9 wt % modified MoS_2 nanosheets results in a 43.3 °C increase in T_{on} and 62.1 °C increase in $T_{50\%}$. On the basis of our previous work, the significant reinforcement of thermal stability may benefit from reduced heat conduction and restricted motion of macromolecules by the MoS_2. The increase in the char residue may be attributed to the capture ability of MoS_2 to the pyrolysis products during the degradation process at high temperature.[39]

DOI: 10.1021/acsami.5b02312
ACS Appl. Mater. Interfaces 2015, 7, 13164−13173

4. CONCLUSIONS

In conclusion, the MoS_2 nanosheets were simultaneously exfoliated and noncovalently functionalized by ultrasonication in a Pluronic aqueous solution. Due to the high content of adsorbed surfactant on the surface of the nanosheets, the MoS_2 obtained could be well redispersed in water and used to prepare the PEO-based nanocomposites. XRD, TEM, and SEM results revealed the homogeneous dispersion of MoS_2 and the strong nanosheet/matrix interfacial adhesion. The incorporation of MoS_2 nanosheets obviously devastated the spherocrystal structure of the PEO matrix and resulted in the morphological alterations, which could be attributed to the molecular level entanglements between PEO chain segments in Pluronic and the bulk PEO molecular chains, the formation of gradient interface, and the enlarged effective volume of MoS_2 nanosheets in the composites. The considerable barrier action of MoS_2 nanosheets could dramatically restrict the ordering of crystal lamellae and the motion of polymer chains as evidenced by the high value of the T_g and superior thermal stability of PEO/MoS_2 nanocomposites. Importantly, the nanoconfined interface region induced by gradient effect could achieve the efficient load transfer from weak chains to robust fillers, thus endowing the PEO/MoS_2 composite films with excellent mechanical strength. Therefore, the formation of the gradient interface region with appropriate rigidity covered on the uniformly distributed nanosheets in the polymer matrix is critically important for enhancing the properties of polymer nanocomposites. This work will enable MoS_2 nanosheets to achieve their maximum potential in polymer nanocomposites.

■ ASSOCIATED CONTENT

Supporting Information

Nonisothermal DSC scans of PEO and its nanocomposites. The Supporting Information is available free of charge on the ACS Publications website at DOI: 10.1021/acsami.5b02312.

■ AUTHOR INFORMATION

Corresponding Authors

*E-mail: yuanhu@ustc.edu.cn. Fax: +86-551-63601664. Tel.: +86-551-63601664.

*E-mail: xingwy@ustc.edu.cn. Fax: +86-551-63601664. Tel.: +86-551-63601664.

Notes

The authors declare no competing financial interest.

■ ACKNOWLEDGMENTS

The work was financially supported by the National Natural Science Foundation of China (No. 21374111, 51203146) and the China Postdoctoral Science Foundation (No. 2013T60621).

■ REFERENCES

(1) Castro-Guerrero, C. F.; Deepak, F. L.; Ponce, A.; Cruz-Reyes, J.; Del Valle-Granados, M.; Fuentes-Moyado, S.; Galvan, D. H.; Jose-Yacaman, M. Structure and Catalytic Properties of Hexagonal Molybdenum Disulfide Nanoplates. *Catal. Sci. Technol.* **2011**, *1*, 1024−1031.

(2) Raybaud, P.; Hafner, J.; Kresse, G.; Kasztelan, S.; Toulhoat, H. Ab Initio Study of the H_2-H_2S/MoS_2 Gas-Solid Interface: the Nature of the Catalytically Active Sites. *J. Catal.* **2000**, *189*, 129−146.

(3) Matte, H. S. S. R.; Gomathi, A.; Manna, A. K.; Late, D. J.; Datta, R.; Pati, S. K.; Rao, C. N. R. MoS_2 and WS_2 Analogues of Graphene. *Angew. Chem., Int. Ed.* **2010**, *49*, 4059−4062.

(4) Rapoport, L.; Fleischer, N.; Tenne, R. Applications of WS_2 (MoS_2) Inorganic Nanotubes and Fullerene-Like Nanoparticles for Solid Lubrication and for Structural Nanocomposites. *J. Mater. Chem.* **2005**, *15*, 1782−1788.

(5) Wahl, K. J.; Singer, I. L. Quantification of a Lubricant Transfer Process that Enhances the Sliding Life of a MoS_2 Coating. *Tribol. Lett.* **1995**, *1*, 59−66.

(6) Kim, S.; Konar, A.; Hwang, W. S.; Lee, J. H.; Lee, J.; Yang, J.; Jung, C.; Kim, H.; Yoo, J. B.; Choi, J. Y.; Jin, Y. W.; Lee, S. Y.; Jena, D.; Choi, W.; Kim, K. High-Mobility and Low-Power Thin-Film Transistors Based on Multilayer MoS_2 Crystals. *Nat. Commun.* **2012**, *3*, 1011.

(7) Xiao, J.; Choi, D. W.; Cosimbescu, L.; Koech, P.; Liu, J.; Lemmon, J. P. Exfoliated MoS_2 Nanocomposite as an Anode Material for Lithium Ion Batteries. *Chem. Mater.* **2010**, *22*, 4522−4524.

(8) Voiry, D.; Salehi, M.; Silva, R.; Fujita, T.; Chen, M. W.; Asefa, T.; Shenoy, V. B.; Eda, G.; Chhowalla, M. Conducting MoS_2 Nanosheets as Catalysts for Hydrogen Evolution Reaction. *Nano Lett.* **2013**, *13*, 6222−6227.

(9) Lukowski, M. A.; Daniel, A. S.; Meng, F.; Forticaux, A.; Li, L. S.; Jin, S. Enhanced Hydrogen Evolution Catalysis from Chemically Exfoliated Metallic MoS_2 Nanosheets. *J. Am. Chem. Soc.* **2013**, *135*, 10274−10277.

(10) Balendhran, S.; Ou, J. Z.; Bhaskaran, M.; Sriram, S.; Ippolito, S.; Vasic, Z.; Kats, E.; Bhargava, S.; Zhuiykov, S.; Kalantar-zadeh, K. Atomically Thin Layers of MoS_2 Via a Two Step Thermal Evaporation-Exfoliation Method. *Nanoscale* **2012**, *4*, 461−466.

(11) Yao, Y. G.; Tolentino, L.; Yang, Z. Z.; Song, X. J.; Zhang, W.; Chen, Y. S.; Wong, C. P. High-Concentration Aqueous Dispersions of MoS_2. *Adv. Funct. Mater.* **2013**, *23*, 3577−3583.

(12) Coleman, J. N.; Lotya, M.; O'Neill, A.; Bergin, S. D.; King, P. J.; Khan, U.; Young, K.; Gaucher, A.; De, S.; Smith, R. J.; Shvets, I. V.; Arora, S. K.; Stanton, G.; Kim, H. Y.; Lee, K.; Kim, G. T.; Duesberg, G. S.; Hallam, T.; Boland, J. J.; Wang, J. J.; Donegan, J. F.; Grunlan, J. C.; Moriarty, G.; Shmeliov, A.; Nicholls, R. J.; Perkins, J. M.; Grieveson, E. M.; Theuwissen, K.; McComb, D. W.; Nellist, P. D.; Nicolosi, V. Two-Dimensional Nanosheets Produced by Liquid Exfoliation of Layered Materials. *Science* **2011**, *331*, 568−571.

(13) Wu, Z. Z.; Wang, D. Z.; Sun, A. K. Preparation of MoS_2 by a Novel Mechanochemical Method. *J. Alloys Compd.* **2010**, *492*, L5−L7.

(14) Feng, X. M.; Wang, X.; Xing, W. Y.; Zhou, K. Q.; Song, L.; Hu, Y. Liquid-Exfoliated MoS_2 by Chitosan and Enhanced Mechanical and Thermal Properties of Chitosan/MoS_2 Composites. *Compos. Sci. Technol.* **2014**, *93*, 76−82.

(15) O'Neill, A.; Khan, U.; Coleman, J. N. Preparation of High Concentration Dispersions of Exfoliated MoS_2 with Increased Flake Size. *Chem. Mater.* **2012**, *24*, 2414−2421.

(16) Ha, H. W.; Choudhury, A.; Kamal, T.; Kim, D. H.; Park, S. Y. Effect of Chemical Modification of Graphene on Mechanical, Electrical, and Thermal Properties of Polyimide/Graphene Nanocomposites. *ACS Appl. Mater. Interfaces* **2012**, *4*, 4623−4630.

(17) Eksik, O.; Gao, J.; Shojaee, S. A.; Thomas, A.; Chow, P.; Bartolucci, S. F.; Lucca, D. A.; Koratkar, N. Epoxy Nanocomposites with Two-Dimensional Transition Metal Dichalcogenide Additives. *ACS Nano* **2014**, *8*, 5282−5289.

(18) Kim, H.; Abdala, A. A.; Macosko, C. W. Graphene/Polymer Nanocomposites. *Macromolecules* **2010**, *43*, 6515−6530.

(19) Ramanathan, T.; Abdala, A. A.; Stankovich, S.; Dikin, D. A.; Herrera-Alonso, M.; Piner, R. D.; Adamson, D. H.; Schniepp, H. C.; Chen, X.; Ruoff, R. S.; Nguyen, S. T.; Aksay, I. A.; Prud'homme, R. K.; Brinson, L. C. Functionalized Graphene Sheets for Polymer Nanocomposites. *Nat. Nanotechnol.* **2008**, *3*, 327−331.

(20) Zhou, K. Q.; Jiang, S. H.; Bao, C. L.; Song, L.; Wang, B. B.; Tang, G.; Hu, Y.; Gui, Z. Preparation of Poly(Vinyl Alcohol) Nanocomposites with Molybdenum Disulfide (MoS_2): Structural Characteristics and Markedly Enhanced Properties. *RSC Adv.* **2012**, *2*, 11695−11703.

(21) Cao, Y. C.; Xu, C. X.; Wu, X.; Wang, X.; Xing, L.; Scott, K. A Poly (Ethylene Oxide)/Graphene Oxide Electrolyte Membrane for

Low Temperature Polymer Fuel Cells. *J. Power Sources* **2011**, *196*, 8377−8382.
(22) Jin, Q.; Schexnailder, P.; Gaharwar, A. K.; Schmidt, G. Silicate Cross-Linked Bio-Nanocomposite Hydrogels from PEO and Chitosan. *Macromol. Biosci.* **2009**, *9*, 1028−1035.
(23) Uyar, T.; Besenbacher, F. Electrospinning of Cyclodextrin Functionalized Polyethylene Oxide (PEO) Nanofibers. *Eur. Polym. J.* **2009**, *45*, 1032−1037.
(24) Zhao, P.; Liu, L. X.; Feng, X. Q.; Wang, C.; Shuai, X. T.; Chen, Y. M. Molecular Nanoworm with PCL Core and PEO Shell as a Non-Spherical Carrier for Drug Delivery. *Macromol. Rapid Commun.* **2012**, *33*, 1351−1355.
(25) Mahmoud, W. E. Morphology and Physical Properties of Poly(Ethylene Oxide) Loaded Graphene Nanocomposites Prepared by Two Different Techniques. *Eur. Polym. J.* **2011**, *47*, 1534−1540.
(26) Feng, X. M.; Wang, X.; Xing, W. Y.; Yu, B.; Song, L.; Hu, Y. Simultaneous Reduction and Surface Functionalization of Graphene Oxide by Chitosan and Their Synergistic Reinforcing Effects in PVA Films. *Ind. Eng. Chem. Res.* **2013**, *52*, 12906−12914.
(27) Quinn, M. D. J.; Ho, N. H.; Notley, S. M. Aqueous Dispersions of Exfoliated Molybdenum Disulfide for Use in Visible-Light Photocatalysis. *ACS Appl. Mater. Interfaces* **2013**, *5*, 12751−12756.
(28) Chrissopoulou, K.; Andrikopoulos, K. S.; Fotiadou, S.; Bollas, S.; Karageorgaki, C.; Christofilos, D.; Voyiatzis, G. A.; Anastasiadis, S. H. Crystallinity and Chain Conformation in PEO/Layered Silicate Nanocomposites. *Macromolecules* **2011**, *44*, 9710−9722.
(29) Zheng, Y.; Bruening, M. L.; Baker, G. L. Crystallization of Polymer Brushes with Poly(Ethylene Oxide) Side Chains. *Macromolecules* **2007**, *40*, 8212−8219.
(30) Zhang, Y. Q.; Xu, H. J.; Yang, J. J.; Chen, S. Y.; Ding, Y. S.; Wang, Z. G. Significantly Accelerated Spherulitic Growth Rates for Semicrystalline Polymers through the Layer-by-Layer Film Method. *J. Phys. Chem. C* **2013**, *117*, 5882−5893.
(31) Layek, R. K.; Kuila, A.; Chatterjee, D. P.; Nandi, A. K. Amphiphilic Poly(N-Vinyl Pyrrolidone) Grafted Graphene by Reversible Addition and Fragmentation Polymerization and the Reinforcement of Poly(Vinyl Acetate) Films. *J. Mater. Chem. A* **2013**, *1*, 10863−10874.
(32) Wang, X.; Xing, W. Y.; Zhang, P.; Song, L.; Yang, H. Y.; Hu, Y. Covalent Functionalization of Graphene with Organosilane and Its Use as a Reinforcement in Epoxy Composites. *Compos. Sci. Technol.* **2012**, *72*, 737−743.
(33) Kulkarni, D. D.; Choi, I.; Singamaneni, S.; Tsukruk, V. V. Graphene Oxide-Polyelectrolyte Nanomembranes. *ACS Nano* **2010**, *4*, 4667−4676.
(34) Bertolazzi, S.; Brivio, J.; Kis, A. Stretching and Breaking of Ultrathin MoS_2. *ACS Nano* **2011**, *5*, 9703−9709.
(35) Chan, C. M.; Wu, J. S.; Li, J. X.; Cheung, Y. K. Polypropylene/Calcium Carbonate Nanocomposites. *Polymer* **2002**, *43*, 2981−2992.
(36) Coleman, J. N.; Cadek, M.; Blake, R.; Nicolosi, V.; Ryan, K. P.; Belton, C.; Fonseca, A.; Nagy, J. B.; Gun'ko, Y. K.; Blau, W. J. High-Performance Nanotube-Reinforced Plastics: Understanding the Mechanism of Strength Increase. *Adv. Funct. Mater.* **2004**, *14*, 791−798.
(37) Qian, X. D.; Yu, B.; Bao, C. L.; Song, L.; Wang, B. B.; Xing, W. Y.; Hu, Y.; Yuen, R. K. K. Silicon Nanoparticle Decorated Graphene Composites: Preparation and Their Reinforcement on the Fire Safety and Mechanical Properties of Polyurea. *J. Mater. Chem. A* **2013**, *1*, 9827−9836.
(38) Yourdkhani, M.; Mousavand, T.; Chapleau, N.; Hubert, P. Thermal, Oxygen Barrier and Mechanical Properties of Polylactide-Organoclay Nanocomposites. *Compos. Sci. Technol.* **2013**, *82*, 47−53.
(39) Feng, X.; Xing, W.; Song, L.; Hu, Y. In Situ Synthesis of a MoS_2/CoOOH Hybrid by a Facile Wet Chemical Method and the Catalytic Oxidation of CO in Epoxy Resin During Decomposition. *J. Mater. Chem. A* **2014**, *2*, 13299−13308.

DOI: 10.1021/acsami.5b02312
ACS Appl. Mater. Interfaces 2015, 7, 13164−13173